PLOS ONE

RESEARCH ARTICLE

In vitro singlet state and zero-quantum encoded magnetic resonance spectroscopy: Illustration with N-acetyl-aspartate

Andrey N. Pravdivtsev[1]*, Frank D. Sönnichsen[2], Jan-Bernd Hövener[1]*

1 Section Biomedical Imaging, Molecular Imaging North Competence Center (MOIN CC), Department of Radiology and Neuroradiology, University Medical Center Kiel, Kiel University, Kiel, Germany, **2** Otto Diels Institute for Organic Chemistry, Kiel University, Kiel, Germany

* andrey.pravdivtsev@rad.uni-kiel.de (ANP); jan.hoevener@rad.uni-kiel.de (JBH)

Citation: Pravdivtsev AN, Sönnichsen FD, Hövener J-B (2020) In vitro singlet state and zero-quantum encoded magnetic resonance spectroscopy: Illustration with N-acetyl-aspartate. PLoS ONE 15(10): e0239982. https://doi.org/10.1371/journal.pone.0239982

Editor: Patrick van der Wel, Rijksuniversiteit Groningen, NETHERLANDS

Received: February 26, 2020

Accepted: September 16, 2020

Published: October 1, 2020

Data Availability Statement: All relevant data are within the manuscript and its Supporting Information files.

Funding: We acknowledge support by the Emmy Noether Program "metabolic and molecular MR" (HO 4604/2-2), the research training circle "materials for brain" (GRK 2154/1-2019), DFG - RFBR grant (HO 4604/3-1, 19-53-12013), the German Federal Ministry of Education and Research (BMBF) within the framework of the e:Med research and funding concept (Try-IBD,

Abstract

Magnetic resonance spectroscopy (MRS) allows the analysis of biochemical processes non-invasively and in vivo. Still, its application in clinical diagnostics is rare. Routine MRS is limited to spatial, chemical and temporal resolutions of cubic centimetres, mM and minutes. In fact, the signal of many metabolites is strong enough for detection, but the resonances significantly overlap, exacerbating identification and quantification. Besides, the signals of water and lipids are much stronger and dominate the entire spectrum. To suppress the background and isolate selected signals, usually, relaxation times, J-coupling and chemical shifts are used. Here, we propose methods to isolate the signals of selected molecular groups within endogenous metabolites by using long-lived spin states (LLS). We exemplify the method by preparing the LLSs of coupled protons in the endogenous molecules N-acetyl-L-aspartic acid (NAA). First, we store polarization in long-lived, double spin states, followed by saturation pulses before the spin order is converted back to observable magnetization or double quantum filters to suppress background signals. We show that LLS and zero-quantum coherences can be used to selectively prepare and measure the signals of chosen metabolites or drugs in the presence of water, inhomogeneous field and highly concentrated fatty solutions. The strong suppression of unwanted signals achieved allowed us to measure pH as a function of chemical shift difference.

1. Introduction

Magnetic resonance (MR) has found a multitude of applications in medical imaging, from anatomy to motion, function and metabolism [1–3]. Likely, one of the most promising, yet least delivering applications is in vivo MR spectroscopy (MRS). MRS provides a non-invasive window into the biochemistry of living organisms–basically a virtual biopsy. Alas, it does not live up to this promise, as MRS is rarely used in routine diagnostics.

In the brain diagnostics, the success of MRS is hampered by the interplay of two major issues: first, a comparatively weak signal of the metabolites of interest, and second,

01ZX1915C), cluster of Excellence "precision medicine in inflammation" (PMI 1267). Kiel University and the Medical Faculty are acknowledged for supporting the Molecular Imaging North Competence Center (MOIN CC) as a core facility for imaging in vivo. MOIN CC was founded by a grant from the European Regional Development Fund (ERDF) and the Zukunftsprogramm Wirtschaft of Schleswig-Holstein (Project no. 122-09-053). The funders had no role in study design, data collection and analysis, decision to publish, or preparation of the manuscript.

Competing interests: The authors have declared that no competing interests exist.

Abbreviations: CW, continuous-wave excitation; LLS, long-lived spin states; MRS, Magnetic resonance spectroscopy; MS, Model Solution; NAA, N-acetyl-L-aspartic acid; OPSYd, Only-Parahydrogen SpectroscopY with double quantum coherence filter; SAR, specific absorption rate; SISTEM, singlet-state encoded magnetic resonance spectroscopy; SM, supporting materials; SUCCESS, suppression of undesired chemicals using contrast-enhancing singlet states.

confounding overlapping resonances and strong background signals mostly from water, lipids and proteins [4]. As a result, most of the time, only highly concentrated metabolites are detected, such as the major brain metabolites N-acetyl-l-aspartic acid (NAA), creatine (Cr), choline (Cho), myo-Inositol (Myo), lactate, alanine and non-exchangeable protons on proteins. For example, up to 0.1% of the brain tissue wet weight of mammals belongs to NAA [5] which is associated with neuronal integrity [6, 7].

^{2}H-enriched, nonradioactive molecules like ^{2}H-glucose are used to obtain background-free spectra in vivo. Valuable insights into biochemistry were gained by this approach [8–10]. However, because of the limited amount of substrate that can be administered in conjunction with the low magnetogyric ratio of ^{2}H, the signal remains low and does not allow routine high-resolution imaging.

Hyperpolarization techniques boost the signal of selected, isotopically labelled metabolites. This way, the fate of a dedicated, polarized agent can be followed in vivo with increased spatial, chemical and temporal resolution [11–13]. For example, hyperpolarization allows imaging the distribution of the hyperpolarized agent, mapping of tissue pH or metabolic conversion [14]. These methods provide different information than conventional MRS without injections, where a quasi-steady state of the metabolism is measured.

In humans, hyperpolarization has shown great promise for imaging prostate cancer, brain cancer, monitoring therapy response, heart metabolism and lung imaging [15–20]. Still, the method is limited by the relatively short lifetime of the signal enhancement and thus short observation window, as well as the limited amount of hyperpolarized agent that can be injected. Additional requirements include a hyperpolarizer, specialized imaging sequences and an X-nuclei channel for the MR system [21–24].

One may argue that the signals of many metabolites are already strong enough for many applications without further enhancement. Unfortunately, it is difficult to isolate the signal of an individual metabolite in the densely packed ^{1}H spectrum of the human brain; the resonances of many interesting metabolites overlap or differ only by a few parts per million. Thus, much inventiveness has gone into the development of suppression and spectral editing techniques [7, 25–32], exploiting differences in chemical shift, relaxation times or J-couplings.

The presence of numerous small molecules, proteins and fat greatly complicates the analysis of a spectrum; all aliphatic protons abundant in fat and small molecules occupy the same chemical shift region of 1–5 ppm. Therefore, usually, only the sharpest singlets or doublet signals of CH_3 protons of small molecules are prominent in ^{1}H-MRS [1, 7, 27, 28].

The use of so-called singlet or long-lived states to improve MRI was suggested before. Often, the singlet state of strongly coupled nuclei is much longer lived (T_{LLS}) than the corresponding longitudinal magnetization (T_1) [33–35]. It was suggested to use such long-lived states (LLS) as a new MR contrast [31, 32, 36], to measure slow diffusion [37, 38] or to track chemical exchange [39]. But the long lifetime is not the single unique property of LLSs. Just as interesting is that broad-band decoupling or continuous-wave excitation (CW) preserve these states and even prolong their lifetime [40], while "normal" resonances are saturated. To get more information from the spectra, the "suppression of (the signal of) undesired chemicals using contrast-enhancing singlet states" (SUCCESS) was proposed by DeVience et al. [41]. During the publication process of this paper, Glöggler et al. [31] proposed a new method for filtering singlet states. Thus far, however, LLS-filtering methods were demonstrated only on high-resolution NMR devices, often with strong radio frequency (RF) power applied.

We suggest to use "singlet-state encoded MR" (SISTEM) as a more general term than SUCCESS and because it reflects the physics of the sequence better than the name of an author (e.g. "Sarkar-II" [39]). Using this terminology, in this paper, we study the properties of SISTEM sequences (**Fig 1**), namely SISTEM-I (former Sarkar-II, **Fig 2A**) and SISTEM-II, a new

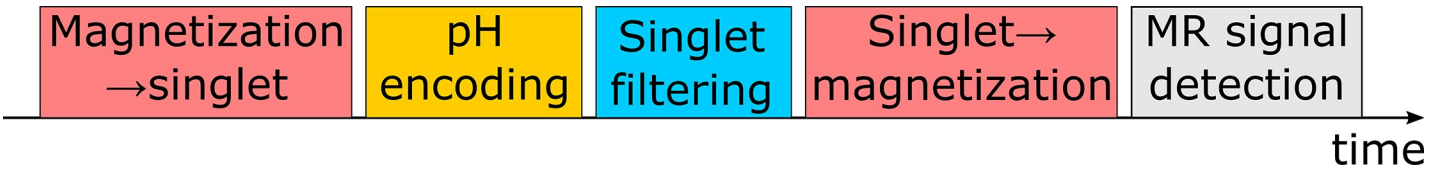

Fig 1. Suggested 5-step SISTEM pulse sequence: (1) magnetization of ^{1}H nuclei is transferred to LLSs and zero-quantum coherences; (2) encoding a feature (here: Chemical shift difference that can be correlated with the pH value, Figs 4 and 5); (3) background suppression: Only singlet spin states (or zero-quantum coherences) pass through the filter; (4) conversion of singlet state into observable magnetization and (5), MR signal detection.

https://doi.org/10.1371/journal.pone.0239982.g001

sequence shown in Fig 4A. We selectively prepared the signal of specific, endogenous metabolites using SISTEM at high-resolution NMR and small-animal MRI unit. SISTEM sequences are modular, broad-band and can require only little RF power deposition. We show that this method may serve purposes beyond background suppression e.g. for pH imaging.

2. Materials and methods

2.1. Chemistry

N-acetyl-l-aspartic acid (NAA, Sigma-Aldrich, 00920, CAS: 997-55-7, Scheme 1), DL-lactic acid (Sigma-Aldrich, 69785, CAS: 50-21-5), l-alanine (Sigma-Aldrich, A7469, CAS: 56-41-7), creatine monohydrate (Sigma-Aldrich, C3630, CAS: 6020-87-7), choline chloride (Sigma-Aldrich, C7017, CAS: 67-48-1), l-glutamic acid (Sigma-Aldrich, 49449, CAS: 56-86-0), myo-Inositol (Sigma-Aldrich, I7508, CAS: 87-89-8) were purchased and used without further purification.

Model solution 1 (MS1). Each of the substrates listed above was dissolved in D_2O (Deutero GmbH, 00506) to yield a concentration of 10 mmol/L. pH was adjusted to the desired value by adding NaOD (Deutero GmbH, 03703) or DCl (Sigma Aldrich, 543047); pH-dependent NMR spectra of all substrates are given in **SM**. Note that only NAA is discussed in the main text.

Model solution 2 (MS2). 300 μL D_2O solution of 10 mmol/L of NAA was mixed with 300 μL food-grade dairy cream (30% fat concentration).

Model solution 3 (MS3). 1500 μL deionized H_2O solution of 100 mmol/L of NAA with a pH 5.15.

2.2. NMR and MRI

All high-resolution NMR spectra were acquired on a 600 MHz vertical bore NMR spectrometer (Bruker Avance II) with a cryogenically cooled probe (TCI) and 5 mm NMR tubes (Wilmad).

Nonlocalized spectra were acquired with a 7 T horizontal bore MRI with a 30 cm diameter of the inner bore (Bruker 7/30 ClinScan), equipped with a ^{1}H transmit-receive volume coil with an inner diameter of 8 cm for excitation and a single loop surface coil with an inner diameter of 0.9 cm for detection [42]. **MS3** was filled into a 1.5 mL container (Eppendorf vial) and placed in the pick-up coil at the isocenter of the magnet. Both NMR and MRI were adjusted using the standard procedures for resonance frequency, shim, flip angle and receiver gain.

Routine nonlocalized spectroscopy and inversion recovery sequences were used; SISTEM-I and -II were implemented using the manufacturer's software (TopSpin 3.2 or Siemens VB15, IDEA 1.5b1.63). The same software was used to process data.

The signals were quantified by integrating amplitude spectra (Fig 4, **S2 Fig in** S1 File).

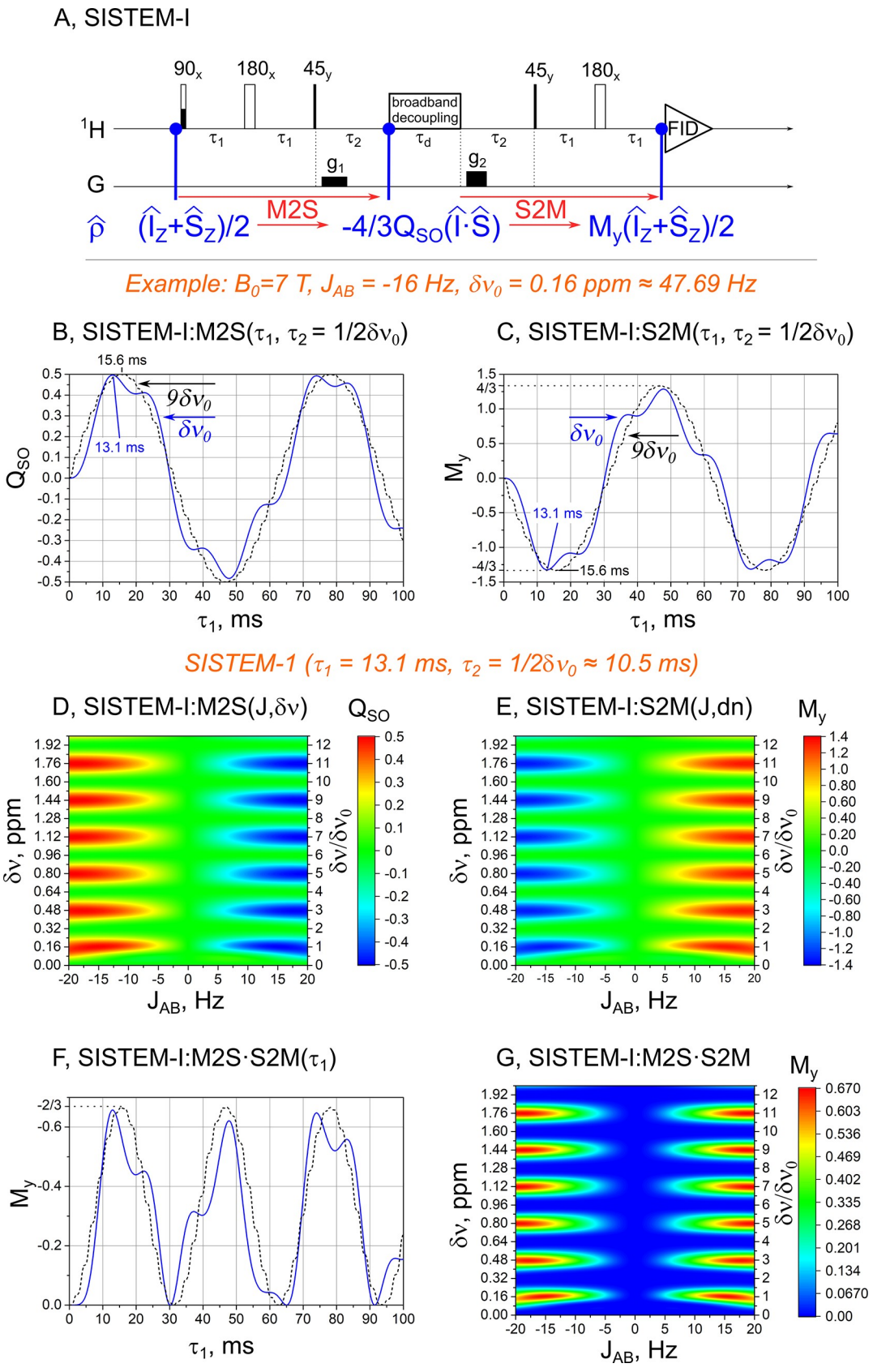
A, SISTEM-I
90x
180x
45y
45y
180x
broadband decoupling
1H
τ1
τ1
τ2
τd
τ2
τ1
τ1
FID
g1
g2
G
M2S
S2M
ρ̂
(Î_Z+Ŝ_Z)/2
-4/3Q_SO(Î·Ŝ)
M_y(Î_Z+Ŝ_Z)/2
Example: B0=7 T, J_AB = -16 Hz, δν0 = 0.16 ppm ≈ 47.69 Hz
B, SISTEM-I:M2S(τ1, τ2 = 1/2δν0)
C, SISTEM-I:S2M(τ1, τ2 = 1/2δν0)
15.6 ms
13.1 ms
9δν0
δν0
Q_SO
M_y
τ1, ms
SISTEM-1 (τ1 = 13.1 ms, τ2 = 1/2δν0 ≈ 10.5 ms)
D, SISTEM-I:M2S(J,δν)
E, SISTEM-I:S2M(J,dn)
Q_SO
M_y
δν, ppm
δν/δν0
J_AB, Hz
F, SISTEM-I:M2S·S2M(τ1)
G, SISTEM-I:M2S·S2M
M_y
τ1, ms
δν, ppm
δν/δν0
J_AB, Hz

Fig 2. Scheme of SISTEM-I (A), its magnetization-to-singlet (M2S) and singlet-to-magnetization (S2M) polarization transfer performance (B-E), and efficacy of the entire sequence (M2S·S2M, F, G). For the AB-type two-spin system investigated ($\delta\nu_0$ = 0.16 ppm, J_{AB} = -16 Hz, θ≅9˚ at B_0 = 7 T, dashed lines in B,C,F), M2S and S2M polarization transfer deviate from the sine-shape, $\sin(2\pi\tau_1 J_{AB})$, predicted for a weakly coupled AX-type two-spin system (here, $\delta\nu = 9\cdot\delta\nu_0$, J_{AB} = -16 Hz, θ ≅1˚, solid lines in B,C,F). [39] Optimal parameters for the AB system are τ_1 = 13.1 *ms* and $\tau_2 = 1/\Delta\nu_0$. In these conditions, "M2S" element provide conversion of 100% magnetization to 50% of singlet-triplet imbalance $\left(\frac{1}{2}\left(\hat{I}_z+\hat{S}_z\right)\right)^{"}M2S^{"\overrightarrow{M2S}} - \frac{4}{3}\left(\hat{\mathrm{I}}\cdot\hat{\mathrm{S}}\right)\cdot \mathrm{Q}_{\mathrm{ST}}$, with Q_{ST} = ½), (D). "S2M" polarization transfer element demonstrates similar behavior (E), here calculation is started with Q_{ST} = 100% $\left(\left(-\frac{4}{3}\left(\hat{\mathrm{I}}\cdot\hat{\mathrm{S}}\right)\right)^{"}S2M^{"\overrightarrow{S2M}}\frac{1}{2}\left(\hat{I}_y+\hat{S}_y\right)\cdot M_y\right.$, with M_y = 4/3)). The maximum signal after SISTEM-I sequence is 2/3 of the initial magnetization $\left(\frac{1}{2}\left(\hat{I}_z+\hat{S}_z\right)\right)^{"}M2S\cdot S2M^{"\overrightarrow{M2S\cdot S2M}}\frac{1}{3}\left(\hat{I}_y+\hat{S}_y\right)$, F,G). The performance of the sequence is high for the two spin-½ systems with |*J*| = 16±4 Hz and chemical shift difference of (2*n*−1)($\delta\nu$+10%) where n is natural number (G). τ_2—intervals can be substituted by Thrippleton–Keeler zero-quantum filter [39, 47] to make the sequence independent of the chemical shift difference.

https://doi.org/10.1371/journal.pone.0239982.g002

2.3. Pulse sequence

In general, SISTEM is composed of five steps with different functions (Fig 1), some of which may occur at the same time.

Step 1: In the first stage, thermal spin magnetization is transferred to the population of the singlet state and zero-quantum coherences (ZQCs). To reach this goal, several methods were proposed [43–46]. We chose the method proposed by Sarkar et al. [39] (Sarkar-II) because it is independent of frequency offsets and uses only hard RF-pulses and gradients. To suppress high order quantum coherences, we added the following spoiler gradient (**Figs 2A and 4A**). To suppress ZQCs one can also add a Thrippleton—Keeler filter too (used in **Fig 3** and **S2 Fig in S1 File**) [39, 47].

Step 2: The second stage is used to encode a dedicated feature (e.g. chemical exchange [39], diffusion [48] or pH). Here, we encode the chemical shift difference of NAA-CH_2 protons by introducing a free evolution interval τ_2 (**Figs 2A** and **4A**). During this stage, the in-phase, $\hat{ZQ}_x = \hat{I}_x\hat{S}_x + \hat{I}_y\hat{S}_y$ and out-of-phase, $\hat{ZQ}_y = \hat{I}_y\hat{S}_x - \hat{I}_x\hat{S}_y$, ZQCs mutually alternate [39, 49]:

$$\hat{ZQ}_x \overrightarrow{2\pi\tau(\nu I\hat{I}z + \nu S\hat{S}z)} \overrightarrow{2\pi\tau(\nu_I\hat{I}_z + \nu_S\hat{S}_z)} \hat{ZQ}_x\cos(2\pi\delta\nu\tau) + \hat{ZQ}_y\sin(2\pi\delta\nu\tau) \quad (1)$$

where ν_I and ν_S are Larmour precession frequencies of two spins I and S and $\delta\nu = \nu_I - \nu_S$ is their chemical shift difference.

Step 3: The goal of the third stage is to suppress the signals from unwanted spins and spin states. We implemented two variants: strong broad-band decoupling on the NMR device (**SISTEM-I, Figs 2A and 3, S2 Fig in S1 File**), and Only-Parahydrogen SpectroscopY with double quantum coherence filter (OPSYd) on the MRI system (**SISTEM-II, Fig 4**) [42, 50]. Note that the deposition of RF energy by OPSYd is much lower than that of decoupling and water/fat saturation. Optional broad-band decoupling, however, not only suppresses background signal but also sustains long-lived singlet spin states. This feature of LLSs offers an additional MRI contrast [32]. An alternative background suppression technique is a specialized singlet spin order filter (T_{00}-filters) [51, 52].

Step 4: During the fourth stage, LLSs and ZQCs are transferred back to observable magnetization. For SISTEM-I, we used the second block of the Sarkar-II sequence ("out of phase echo" block, **Fig 2A**). For SISTEM-II, this function is accomplished with OPSYd (**Fig 4A**).

Step 5: During the final stage, MR signal is acquired e.g. by pulse-acquisition experiments or, possibly, imaging.

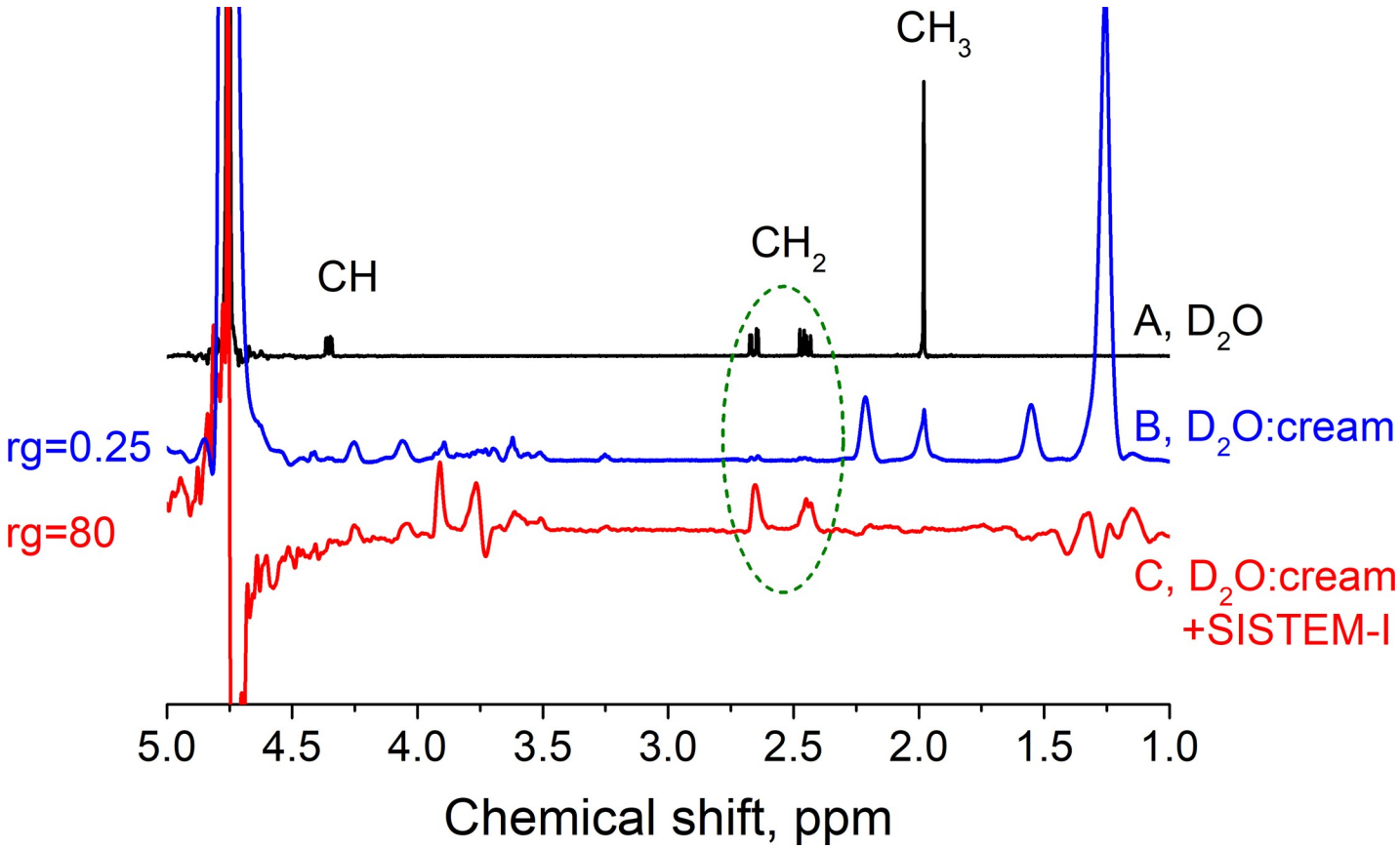

Fig 3. ^{1}H NMR spectra of NAA in D_2O (MS1) and homogeneous field (A), NAA in aqueous-cream solution (MS2) with poor field homogeneity (B) and same solution acquired by SISTEM-I (C). Water (4.7 ppm) and lipid resonances (0.9–2.2 ppm range) [57] dominated the routine NMR spectrum (B) were effectively suppressed by SISTEM-I (C), allowing to increase the receiver gain 320 fold. The NAA-CH_2 resonance was well prepared by SISTEM-I (dashed oval). Interestingly, two other resonances at ≈ 3.8 ppm were also prepared by SISTEM-I. These chemical shifts coincide well with those of D-lactose β (CH_2: 3.96 ppm and 3.81 ppm) [56]. Parameters of SISTEM-I: τ_1 = 8 ms, τ_d = 1 s, number of scans, NS, was 8, no phase cycling, WALTZ-16 decoupling with 2.5 kHz RF- amplitude. ZQCs were suppressed with CHIRP pulses accompanied by gradients [39, 47]. Spectra (A) and (B) were acquired with NS = 1. Average SNR of NAA-CH_2 signals was 23 (B) and 50 (C) for the given parameters and exponential line broadening of 5 Hz.

https://doi.org/10.1371/journal.pone.0239982.g003

3. Results

3.1. Properties of the filter

The performance of SISTEM-I (Fig 2A) (known as "Sarkar-II") is described in Ref. [39] and (**SM**). Again, this pulse sequence was chosen without modifications from Ref. [39] and it seems to be the most simplest, transmitting frequency independent, broadband singlet spin order selecting pulse sequence. The interval τ_1 selects systems with the desired J-coupling constant, J_{AB}, and the interval τ_2 selects the system with the desired chemical shift difference, $\delta\nu$, as the maximum magnetization to singlet order transfer and back occurs for $\tau_1 = \frac{1}{4|J|}$ and $\tau_2 = \frac{1}{\delta\nu}$ (Fig 2B and 2C).

In the first part of SISTEM-I ("M2S"), for a weakly coupled two spin system, the Boltzmann polarization or magnetization is transferred to a singlet-triplet population imbalance, $Q_{SO} = \langle \hat{Q}_{SO} \rangle = \langle -\frac{4}{3}(\hat{S} \cdot \hat{I}) \rangle$ [53], according to the following, simple equation:

$$Q_{S0} = \frac{1}{4}\sin(2\pi J\tau_1)[1 - \cos(2\pi\delta\nu\tau_2)]. \quad (2)$$

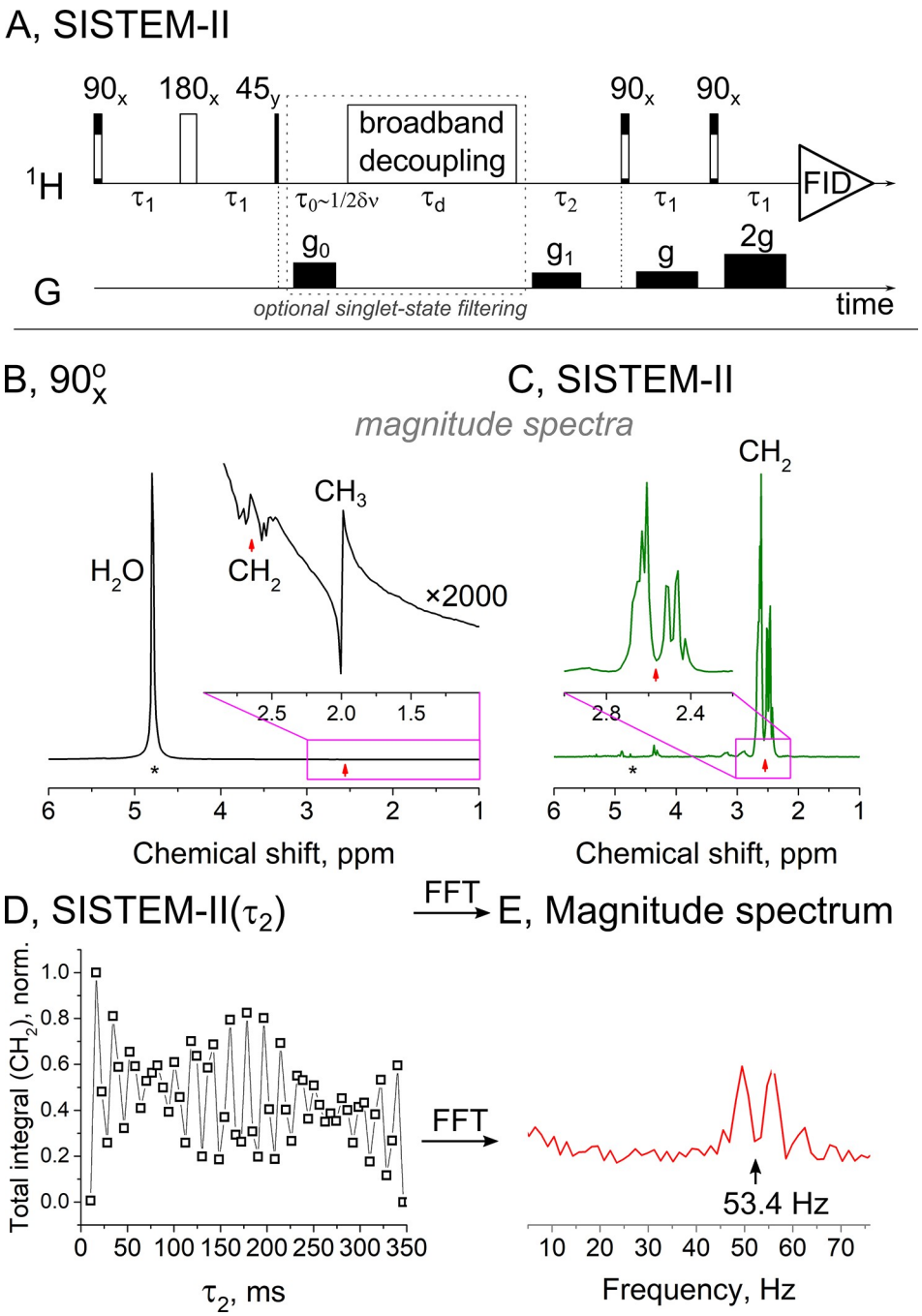

Fig 4. Performance of SISTEM-II on a 7 T MRI and measurement of chemical shift difference and J-coupling constants in inhomogeneous field of MRI. Schematic view of SISTEM-II (A). Optional in this case broadband decoupling (part in the dashed box) was omitted in experiments to decrease SAR (τ_0, $\tau_d = 0$). In comparison to a pulse-acquisition magnitude spectrum (B), the water signal of **MS3** was strongly suppressed by SISTEM-II, while the NAA-CH_2 signal was maintained (C, magnitude, $\tau_1 = 12$ *ms*, $\tau_2 = 8.2$ *ms*). Note that the spectrum has a complex shape, that does not allow to determine $\Delta\delta_{CH_2}$ directly. Instead, the chemical shift difference $\Delta\delta_{CH_2}$ was encoded into the signal by variation of τ_2, and determined by Fourier transforming the summed amplitudes of the SISTEM-II signal acquired for different τ_2 (D). A well-resolved doublet at $\Delta\delta_{CH_2} = 52.7 \pm 0.6$ Hz or ≈0.176±0.002 ppm with the splitting of $\Delta J = J^{CH}_{CH^a_2} - J^{CH}_{CH^b_2} \approx 6.2 \pm 0.6$ Hz was obtained (E) despite a poor field homogeneity (worse than 30 Hz linewidth). Inserts show NAA-CH_2 resonances (B, C). Small red arrows indicate the center of NAA-CH_2 resonances. SISTEM-II experimental time is 5 s for a single scan (C); 55 points (D) were acquired in 4.5 minutes. NAA/background signal in (B) is $\approx 10^{-4}$ and ≈10 in (C). Average SNR of NAA-CH_2 signals was 300 (B) and 1300 (C) for the given experimental parameters.

https://doi.org/10.1371/journal.pone.0239982.g004

However, already for 2-spin systems in the intermediate coupling regime, the matter becomes more complicated, and the polarization transfer behavior deviates from this simple equation (Fig 2B, 2C and 2F). We exemplified the matter with two spin systems with $\theta = \frac{1}{2}Arctan\left(\left|\frac{J}{\delta\nu}\right|\right) \cong 9^{o}$ (AB type) and $\theta \cong 1^{o}$ (AX type). The angle θ tends to zero, $\theta \rightarrow 0$, when the system is weakly coupled (AX type), on the other hand, when $\theta \rightarrow 45^{o}$ the system is considered to be strongly coupled (AB or even A_2 type). A $\theta \cong 9^{\circ}$ corresponds to two NAA-CH_2 protons at pH 5 (**S1 Table in** S1 File).

DeVience et al [44] demonstrated that the intervals τ_1 and τ_2 can be chosen such that almost perfect suppression of NAA is achieved, while signals of aspartate are preserved. Here, we found other feature of this filter: periodic filtration (Fig 2D, 2E and 2G).

First, we optimized the parameters of SISTEM-I for the maximum retained signal of NAA (Fig 2B and 2C) after signal filtration. Then we applied this pulse sequence to other two-spin systems with various chemical shift differences and J-coupling constants (Fig 2D and 2E). As one can see, and it follows from Eq 3, the pulse sequence is insensitive to the sign of J-coupling constant (the sign of the signal is irrelevant in this case), and systems with odd multiples of chemical shift difference pass through the filter. The criteria for the AX systems, that pass through the SISTEM-I filter, follow from Eq 2 and Fig 2:

$$J = (2i+1)J_0, \text{ with } i \in \mathbb{Z}, \text{ and } \tau_1 = \frac{1}{4|J_0|} \tag{3}$$

$$|\delta\nu| = (2n+1)|\delta\nu_0|, \text{ with } n \in \mathbb{N}, \text{ and } \tau_2 = \frac{1}{2\delta\nu_0} \tag{4}$$

Thus, the pulse sequence not only suppresses uncoupled spins like H_2O, but also two spin systems that do not satisfy these criteria (Eqs 3 and 4). Put differently, the SISTEM-I filter is not specific to a single set of J and $\delta\nu$, but to multiples of it as well. The calculation of SISTEM-I performance for the 3 spin system of NAA is given in Supporting Materials.

Free evolution intervals τ_2 (Fig 2A) can be substituted by broad-band CHIRP pulses accompanied by gradients, i.e. by Thrippleton–Keeler filter that suppresses ZQCs [47]. In this case, the pulse sequence is insensitive to the chemical shift difference [39]. We used this approach in our high-resolution NMR experiments (Fig 3, **S2 Fig in** S1 File).

3.2. Implementation of SISTEM-I on a high-resolution NMR spectrometer

It should be noted that SISTEM-I was designed with a 2-spin-½ system in mind [39], however, it can also be applied to three- and multi-spin systems [54]. NAA is effectively a 3 spin-½ system (CH-CH_2, S1 Scheme), therefore the efficiency of the sequence was reduced. For NAA at pH 5, the maximum retained thermal magnetization after SISTEM-I is predicted to be 0.45 (**S1 Fig in** S1 File), while for the two-spin system it is 2/3 (Fig 2). An optimal $\tau_1 \approx$ 12 ms was found for NAA-CH_2 protons and SISTEM-I sequence (**S2 Fig in** S1 File).

Still, the LLS was successfully populated, and the lifetime of $T_{LLS} \approx 6.5$ s was almost 6 times longer than $T_1 \approx 1$ s (**S2 Fig in** S1 File, at 14.1 T with 2.5 kHz WALTZ-16 decoupling [55]). However, note, we do not use the long live-time hereafter as a contrast.

3.3. Suppression of water and fat signals with SISTEM-I on a high-resolution NMR spectrometer

Next, we used a 1:1 mixture of water and dairy cream with 30% fat content (**MS2**, Fig 3B and 3C). To evaluate the performance of the method in a field with poor homogeneity, we

refrained from shimming. The resulting linewidth was irregular with a full width at half maximum of ≈ 30 Hz, resembling in vivo conditions.

As expected, the spectrum of a standard, 90˚ pulse-acquisition experiment (without any suppression techniques) was dominated by fat and water resonances, while only very little NAA was apparent (Fig 3B). Using SISTEM-I, however, the fat and water signals were strongly suppressed, allowing to increase the receiver gain (rg) 320 times (linear, Fig 3C).

The SISTEM-I spectrum showed well-resolved resonances of NAA-CH_2, but no signal from the NAA-CH_3 group, which normally dominates the NAA spectrum. Besides, some water signal and some residues of lipid-$(CH_2)_n$ were found at ≈ 1.3 ppm. The signals in the range 3.5–4.5 ppm were tentatively attributed to lactose; two remained peaks at 3.9 and 3.76 ppm were attributed to CH_2 protons of D-lactose β (3.96 ppm and 3.81 ppm) [56]. Because of similar structure and similar NMR-parameters this pair of spins could pass through the SISTEM-I filter.

3.4. SISTEM-II on a 7 T small animal MRI system

For in vivo applications, care must be taken when using decoupling because much energy may be deposited into the tissue. To circumvent this issue, we propose to use OPSYd filter instead of decoupling (SISTEM-II, Fig 4A). Note that in this case, an additional magnetization to singlet transfer stage is no longer required: OPSYd effect on zero-quantum coherences and LLS is described in **SM**.

We implemented SISTEM-II on a preclinical 7 T MRI. Again, the spectrum of a standard pulse-acquisition method was dominated by water signal three orders of magnitude larger than that of NAA (**MS3**). Water and NAA-CH_3 signals were strongly suppressed by SISTEM-II, while NAA-CH_2 signals were retained (Fig 4B and 4C). Note, that the shape of the resonance is complex and not straight forward to interpret, however, the chemical shift difference, $\Delta\delta_{CH_2}$, still can be measured indirectly.

We used SISTEM-II to encode the chemical shift difference of NAA-CH_2 protons ($\Delta\delta_{CH_2}$) in the magnitude of the SISTEM-II signal as a function of τ_2; other unwanted resonances were suppressed (Fig 4).

To achieve this, we took advantage of the fact that the evolution of the ZQCs during the encoding phase of SISTEM-II depend on $\Delta\delta_{CH_2}$ (Eqs 1 and 2). Thus, by variation of τ_2 and Fourier transform of the resulting signal, we found a doublet centred at $\Delta\delta_{CH_2} = 52.7 \pm 0.6$ Hz (at 7 T or 0.176 ppm). The splitting was caused by an additional modulation of the SISTEM-II signal induced by spin-spin coupling with a third nucleus, the NAA-CH proton (Fig 4E). This splitting equals to 6.2±0.6 *Hz* and corresponds to $\Delta J = J^{CH}_{CH_2^a} - J^{CH}_{CH_2^b}$ (**S1 Table in** S1 File) [58, 59]. Note that it is impossible to determine these parameters with this precision by MRI in a simple pulse-acquisition experiment with a common in MRI magnetic field homogeneity worse than 30 Hz.

Note, that here we did not apply an optional in this case broadband decoupling (Fig 4A) to preserve a singlet spin state as it was done in SISTEM-I, as a result, the singlet spin state is only transient state in the interval τ_2. The broadband decoupling (singlet state filtering) could improve background suppression, albeit by reducing the NMR signal and increasing specific absorption (SAR).

3.5. pH measurement with SISTEM-II on a 7 T small animal MRI system

In general, selectively preparing specific resonances and suppressing background often opens the door for new applications. Now that the chemical shift difference of NAA-CH_2 can be

measured much more precisely than the poor homogeneity of the magnetic field would normally allow, we can use this information to assign the pH of the sample. For this purpose, we acquired seven high-resolution NMR reference spectra of NAA at pH 3–10. $\Delta\delta_{CH_2}$ was found to collapse for low pH approaching 2, and to reach a maximum for a pH of 7 or more ($\approx$ 0.2 ppm, **Fig 5**). According to these data, the $\Delta\delta_{CH_2} = 52.7 \pm 0.6$ Hz measured in the 7 T MRI corresponds to a pH of 5.21±0.05. This finding compares well with the pH value of 5.15 measured with an electrode.

The method does not require any external reference, nor is any correction of magnetic field homogeneity or susceptibility needed, because the chemical shift difference, $\Delta\delta_{CH_2}$, within one and the same molecule is used as a pH meter [60, 61]. Unfortunately, though, for NAA, most of the $\Delta\delta_{CH_2}$ variation is just below the most interesting physiological range of pH. Still, other molecules with more appropriate properties may be identified. Note, that the effect of ionic strength and temperature on correlation of pH value with NMR parameters for the chosen target molecules has to be also considered [62].

4. Discussion

Among the multitude of applications suggested for LLS, we showed here that LLS can be used to selectively prepare the signals of a metabolite, NAA, in the presence of water, inhomogeneous magnetic fields and highly concentrated fatty solutions. This facilitates quantification because the background is greatly suppressed.

One application of this technique may be the measurement of endogenous brain metabolites, either of a whole-brain at once [7] or as a part of localized spectroscopy or imaging methods. Another application may be imaging of biodistribution of drugs. An example would be ethosuximide (ETX, Zarontin) [64], a medication used to treat absence seizures. ETX has an isolated CH_2 group of the two weakly coupled protons, which is ideal for SISTEM-I (**Fig 2**). In this case, up to 2/3 of the thermal Boltzmann signal could be observed. Here, the utility of the method was demonstrated on a three spin-½ system of NAA with two CH_2 protons in the intermediate coupling regime.

SISTEM is not limited to CH_2 groups only, one can exploit other fragments such as CH-CH_3 or other coupled spins [41]. The spin system of lactate (abundant metabolite) e.g., comprises a weakly coupled CH-CH_3 group of spins with J-coupling constant of 7 Hz; in this case, up to 1/3 of the Boltzmann signal can be observed with SISTEM-I.

Nowadays, numerous pulse sequences exist, including recently proposed broad-band generalized magnetization-to-singlet-order transfer [65]. The optimum performance of such sequences covers a significant range of coupled spin systems. The molecule of choice, available equipment and SAR will dictate the use of the filtering method.

It is worth to mention that although double quantum and zero quantum (DQ/ZQ) filters are used in MRS [66] the SISTEM approach is quite different. LLS filtering techniques select not only multi-spin systems but the systems with the specific values of chemical shift and J-coupling constant (**Fig 2**).

Besides imaging the distribution and measuring the concentration of molecules, SISTEM may be used to improve the ability of NMR to probe various tissue properties such as pH. The approach presented here is particularly advantageous because it is independent of the magnetic field homogeneity and requires no external reference. It was already suggested to use heteronuclear (^{31}P, ^{13}C, ^{15}N, e.g.) J-coupling constants and chemical shifts to determine pH value by MRI [61, 62, 67]. X-nuclei methods benefit from little to no background, while ^{1}H methods offer a high detection sensitivity and do not require X-nuclear capabilities.

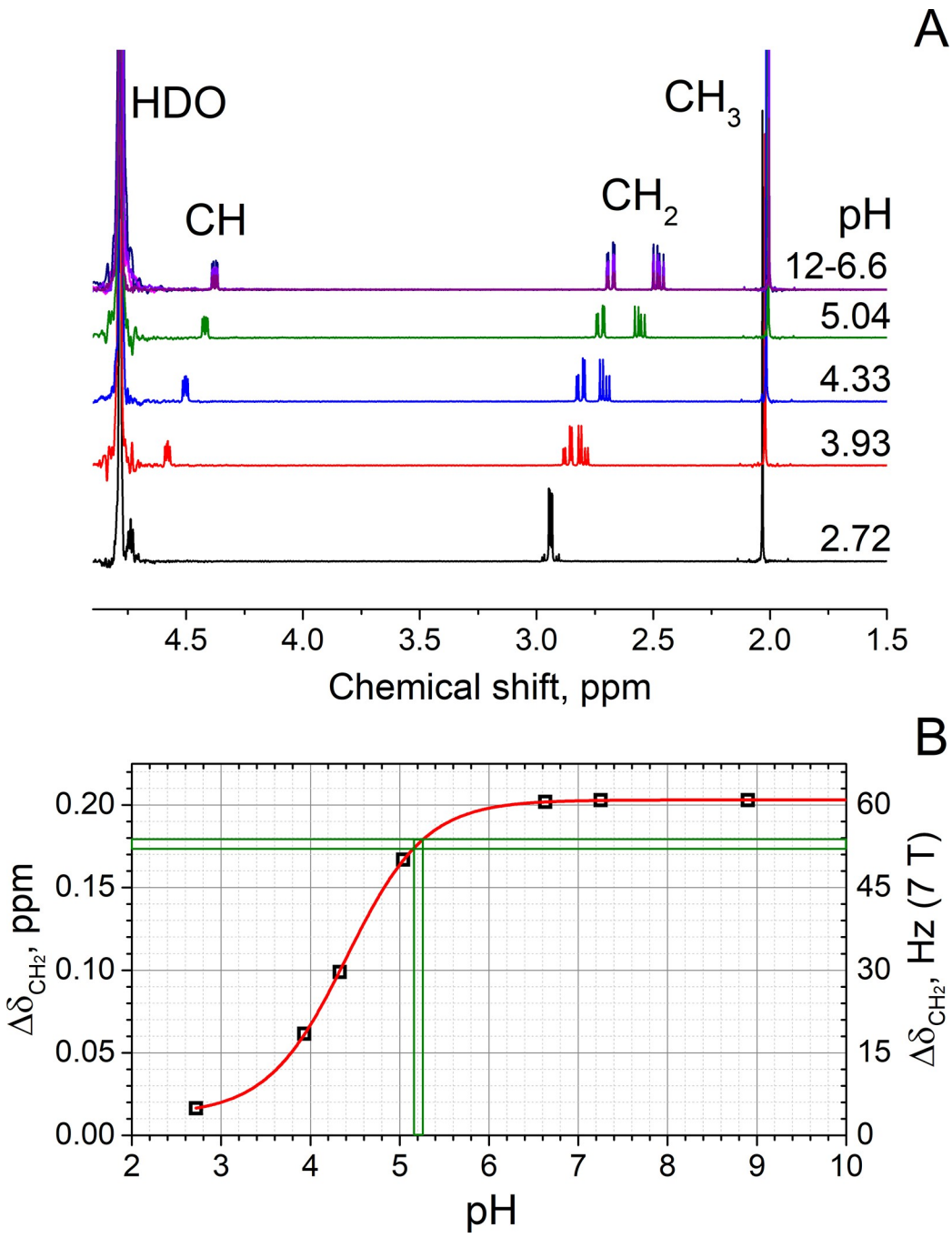

Fig 5. NAA NMR spectra and $\Delta\delta_{CH_2}$ of NAA-CH2 as a function of pH. Seven high resolution, ^{1}H NMR spectra (A) of **MS1** with different pH were acquired to determine the effect of pH on $\Delta\delta_{CH_2}$ (B). Henderson-Hasselbalch equation in a form: $\Delta\delta_{obs} = \Delta\delta_p + \frac{\Delta\delta}{1+10^{pKa-pH}}$ [63] with $\Delta\delta_p$ = 0.013±0.0006 ppm, $\Delta\delta$ = 0.19±0.0006 ppm, pKa = 4.407±0.006 (B, line) was fitted to the data (B, squares). The $\Delta\delta_{CH_2} = 52.7 \pm 0.6$ Hz determined by SITEMS-II (Fig 4E) corresponded to a pH of 5.21±0.05 (cross-section of two green boxes), which corresponded well to the value measured by electrode 5.15. Fitted chemical shifts and J-coupling constants as a function of pH are listed given in **SM** together with fitting parameters.

https://doi.org/10.1371/journal.pone.0239982.g005

While the conditions investigated here were used to approach the situation in vivo, obviously, only in vitro experiments were presented here. If the method has any value for in vivo

biomedical applications has yet to be shown. Still, these first results are promising. We are currently trying to bring together this spectral editing technique with spatial encoding MRI methods (PRESS, CSI, e.g.) to approach with this method in vivo and possibly clinical applications and to assess the gained SNR.

5. Conclusion

We showed that SISTEM can be used to selectively prepare and measure the signals of chosen metabolites or drugs in the presence of water, highly concentrated fatty solutions in homogenous and inhomogeneous fields. Very strong suppression of unwanted signals was observed on an NMR and MRI system with low RF-power deposition (no saturation pulses were used in MRI) that is beneficial for in vivo MRI. The chemical shift difference of the NAA-CH_2 protons was encoded into the SISTEM signal and used for measuring pH. The sequences greatly suppress all isolated/uncoupled protons (e.g. some CH_3 groups, water), however, some multi-spin systems can still pass the filter. In vivo tests are required to see if this method has a biomedical relevance.

Supporting information

S1 File. NMR spectra of all substrates listed in the methods and chemical shifts and J-coupling values for NAA as a function of pH.
(PDF)

S1 Data.
(ZIP)

S1 Scheme. Chemical structure of N-acetyl-l-aspartic acid (NAA). The methyl protons (a, b) were used for SISTEM. The protons have J-coupling constant of 16–17 Hz with a chemical shift of 2.5–3 ppm depending on pH (**SM**).
(TIF)

Author Contributions

Conceptualization: Andrey N. Pravdivtsev.

Formal analysis: Andrey N. Pravdivtsev.

Funding acquisition: Jan-Bernd Hövener.

Investigation: Andrey N. Pravdivtsev.

Methodology: Andrey N. Pravdivtsev.

Resources: Frank D. Sönnichsen, Jan-Bernd Hövener.

Software: Frank D. Sönnichsen.

Supervision: Jan-Bernd Hövener.

Visualization: Andrey N. Pravdivtsev.

Writing – original draft: Andrey N. Pravdivtsev, Jan-Bernd Hövener.

Writing – review & editing: Andrey N. Pravdivtsev, Frank D. Sönnichsen, Jan-Bernd Hövener.

References

1. Robin A. de Graaf. In Vivo NMR Spectroscopy: Principles and Techniques [Internet]. Second edition. Wiley; 2014 [cited 2018 Oct 18]. Available from: https://www.onlinelibrary.wiley.com/doi/abs/10.1002/9780470512968.ch2
2. McRobbie DW, Moore EA, Graves MJ, Prince MR. MRI from Picture to Proton. Cambridge University Press; 2006.
3. Xu V, Chan H, Lin AP, Sailasuta N, Valencerina S, Tran T, et al. MR Spectroscopy in Diagnosis and Neurological Decision-Making. Semin Neurol. 2008; 28(4):407–22. https://doi.org/10.1055/s-0028-1083685 PMID: 18843570
4. Brown FF, Campbell ID, Kuchel PW. Human erythrocyte metabolism studies by 1H spin echo NMR. FEBS Lett. 1977; 82(1):12–6. https://doi.org/10.1016/0014-5793(77)80875-2 PMID: 21099
5. Tallan HH. Studies on the distribution of N-acetyl-L-aspartic acid in brain. J Biol Chem. 1957 Jan; 224 (1):41–5. PMID: 13398385
6. Ross B, Bluml S. Magnetic resonance spectroscopy of the human brain. Anat Rec. 2001; 265(2):54–84. https://doi.org/10.1002/ar.1058 PMID: 11323770
7. Rigotti DJ, Inglese M, Gonen O. Whole-Brain N-Acetylaspartate as a Surrogate Marker of Neuronal Damage in Diffuse Neurologic Disorders. Am J Neuroradiol. 2007 Nov 1; 28(10):1843–9. https://doi.org/10.3174/ajnr.A0774 PMID: 17921226
8. Feyter HMD, Behar KL, Corbin ZA, Fulbright RK, Brown PB, McIntyre S, et al. Deuterium metabolic imaging (DMI) for MRI-based 3D mapping of metabolism in vivo. Sci Adv. 2018 Aug 1; 4(8):eaat7314. https://doi.org/10.1126/sciadv.aat7314 PMID: 30140744
9. McDouall JBL, Evelhoch JL. Deuterium Nuclear Magnetic Resonance Imaging of Tracer Distribution in D2O Clearance Measurements of Tumor Blood Flow in Mice. Cancer Res. 1990 Jan 15; 50(2):363–9. PMID: 2153050
10. Kreis F, Wright AJ, Hesse F, Fala M, Hu D, Brindle KM. Measuring Tumor Glycolytic Flux in Vivo by Using Fast Deuterium MRI. Radiology. 2019 Dec 10; 294(2):289–96. https://doi.org/10.1148/radiol.2019191242 PMID: 31821119
11. Kovtunov KV, Pokochueva E, Salnikov O, Cousin S, Kurzbach D, Vuichoud B, et al. Hyperpolarized NMR: d-DNP, PHIP, and SABRE. Chem Asian J. 2018; 13(15):1857–71.
12. Hövener J-B, Pravdivtsev AN, Kidd B, Bowers CR, Glöggler S, Kovtunov KV, et al. Parahydrogen-Based Hyperpolarization for Biomedicine. Angew Chem Int Ed. 2018 Aug 27; 57(35):11140–62.
13. Kurhanewicz J, Vigneron DB, Ardenkjaer-Larsen JH, Bankson JA, Brindle K, Cunningham CH, et al. Hyperpolarized 13C MRI: Path to Clinical Translation in Oncology. Neoplasia. 2019 Jan 1; 21(1):1–16. https://doi.org/10.1016/j.neo.2018.09.006 PMID: 30472500
14. Hundshammer C, Düwel S, Schilling F. Imaging of Extracellular pH Using Hyperpolarized Molecules. Isr J Chem. 2017 Sep 1; 57(9):788–99.
15. Schröder L, Lowery TJ, Hilty C, Wemmer DE, Pines A. Molecular Imaging Using a Targeted Magnetic Resonance Hyperpolarized Biosensor. Science. 2006 Oct 20; 314(5798):446–9. https://doi.org/10.1126/science.1131847 PMID: 17053143
16. Day SE, Kettunen MI, Gallagher FA, Hu D-E, Lerche M, Wolber J, et al. Detecting tumor response to treatment using hyperpolarized 13C magnetic resonance imaging and spectroscopy. Nat Med. 2007 Nov; 13(11):1382–7. https://doi.org/10.1038/nm1650 PMID: 17965722
17. Boumezbeur F, Petersen KF, Cline GW, Mason GF, Behar KL, Shulman GI, et al. The Contribution of Blood Lactate to Brain Energy Metabolism in Humans Measured by Dynamic 13C Nuclear Magnetic Resonance Spectroscopy. J Neurosci. 2010 Oct 20; 30(42):13983–91. https://doi.org/10.1523/JNEUROSCI.2040-10.2010 PMID: 20962220
18. Dregely I, Ruset IC, Mata JF, Ketel J, Ketel S, Distelbrink J, et al. Multiple-exchange-time xenon polarization transfer contrast (MXTC) MRI: Initial results in animals and healthy volunteers. Magn Reson Med. 2012 Apr 1; 67(4):943–53. https://doi.org/10.1002/mrm.23066 PMID: 22213334
19. Nelson SJ, Kurhanewicz J, Vigneron DB, Larson PEZ, Harzstark AL, Ferrone M, et al. Metabolic Imaging of Patients with Prostate Cancer Using Hyperpolarized [1-13C]Pyruvate. Sci Transl Med. 2013 Aug 14; 5(198):198ra108–198ra108. https://doi.org/10.1126/scitranslmed.3006070 PMID: 23946197
20. Cunningham CH, Lau JYC, Chen AP, Geraghty BJ, Perks WJ, Roifman I, et al. Hyperpolarized 13C Metabolic MRI of the Human Heart. Circ Res. 2016 Nov; 119(11):1177–1182. https://doi.org/10.1161/CIRCRESAHA.116.309769 PMID: 27635086
21. Ardenkjær-Larsen JH, Fridlund B, Gram A, Hansson G, Hansson L, Lerche MH, et al. Increase in signal-to-noise ratio of >10,000 times in liquid-state NMR. PNAS. 2003 Sep 2; 100(18):10158–63. https://doi.org/10.1073/pnas.1733835100 PMID: 12930897

22. Mugler JP, Driehuys B, Brookeman JR, Cates GD, Berr SS, Bryant RG, et al. MR imaging and spectroscopy using hyperpolarized 129Xe gas: Preliminary human results. Magn Reson Med. 2005; 37(6):809–15.

23. Perman WH, Bhattacharya P, Leupold J, Lin AP, Harris KC, Norton VA, et al. Fast volumetric spatial-spectral MR imaging of hyperpolarized 13C-labeled compounds using multiple echo 3D bSSFP. Magn Reson Imaging. 2010 May; 28(4):459–65. https://doi.org/10.1016/j.mri.2009.12.003 PMID: 20171034

24. Kishimoto S, Brender JR, Crooks DR, Matsumoto S, Seki T, Oshima N, et al. Imaging of glucose metabolism by 13C-MRI distinguishes pancreatic cancer subtypes in mice. DeBerardinis R, editor. eLife. 2019 Aug 13; 8:e46312. https://doi.org/10.7554/eLife.46312 PMID: 31408004

25. Ogg RJ, Kingsley RB, Taylor JS. WET, a T1- and B1-Insensitive Water-Suppression Method for in Vivo Localized 1H NMR Spectroscopy. J Magn Reson B. 1994 May 1; 104(1):1–10. https://doi.org/10.1006/jmrb.1994.1048 PMID: 8025810

26. Spielman DM, Pauly JM, Macovski A, Glover GH, Enzmann DR. Lipid-suppressed single-and multisection proton spectroscopic imaging of the human brain. J Magn Reson Imaging. 1992; 2(3):253–62. https://doi.org/10.1002/jmri.1880020302 PMID: 1627859

27. Hövener J-B, Rigotti DJ, Amann M, Liu S, Babb JS, Bachert P, et al. Whole-Brain N-Acetylaspartate MR Spectroscopic Quantification: Performance Comparison of Metabolite versus Lipid Nulling. Am J Neuroradiol [Internet]. 2008 Jun 12 [cited 2018 Feb 6]; Available from: http://www.ajnr.org/content/early/2008/06/12/ajnr.A1171

28. Mullins PG, McGonigle DJ, O'Gorman RL, Puts NAJ, Vidyasagar R, Evans CJ, et al. Current practice in the use of MEGA-PRESS spectroscopy for the detection of GABA. NeuroImage. 2014 Feb 1; 86:43–52. https://doi.org/10.1016/j.neuroimage.2012.12.004 PMID: 23246994

29. Xu S, Ji Y, Chen X, Yang Y, Gullapalli RP, Masri R. In vivo high-resolution localized 1H MR spectroscopy in the awake rat brain at 7 T. Magn Reson Med. 2013; 69(4):937–43. https://doi.org/10.1002/mrm.24321 PMID: 22570299

30. Chen X, Lin M, Chen Z, Cai S, Zhong J. High-resolution intermolecular zero-quantum coherence spectroscopy under inhomogeneous fields with effective solvent suppression. Phys Chem Chem Phys. 2007 Nov 28; 9(47):6231–40. https://doi.org/10.1039/b709154k PMID: 18046472

31. Mamone S, Rezaei-Ghaleh N, Opazo F, Griesinger C, Glöggler S. Singlet-filtered NMR spectroscopy. Sci Adv. 2020 Feb 1; 6(8):eaaz1955. https://doi.org/10.1126/sciadv.aaz1955 PMID: 32128422

32. Kiryutin AS, Zimmermann H, Yurkovskaya AV, Vieth H-M, Ivanov KL. Long-lived spin states as a source of contrast in magnetic resonance spectroscopy and imaging. Journal of Magnetic Resonance. 2015 Dec 1; 261(Supplement C):64–72. https://doi.org/10.1016/j.jmr.2015.10.004 PMID: 26529204

33. Carravetta M, Johannessen OG, Levitt MH. Beyond the T1 Limit: Singlet Nuclear Spin States in Low Magnetic Fields. Phys Rev Lett. 2004 Apr 14; 92(15):153003. https://doi.org/10.1103/PhysRevLett.92.153003 PMID: 15169282

34. Levitt MH. Singlet Nuclear Magnetic Resonance. Annu Rev Phys Chem. 2012; 63(1):89–105.

35. Stevanato G, Hill-Cousins JT, Håkansson P, Roy SS, Brown LJ, Brown RCD, et al. A Nuclear Singlet Lifetime of More than One Hour in Room-Temperature Solution. Angew Chem Int Ed. 2015 Mar 16; 54(12):3740–3.

36. Kiryutin AS, Pravdivtsev AN, Yurkovskaya AV, Vieth H-M, Ivanov KL. Nuclear Spin Singlet Order Selection by Adiabatically Ramped RF Fields. J Phys Chem B. 2016 Nov 23; 120(46):11978–86. https://doi.org/10.1021/acs.jpcb.6b08879 PMID: 27786476

37. C. Tourell M, Pop I-A, J. Brown L, D. Brown RC, Pileio G. Singlet-assisted diffusion-NMR (SAD-NMR): redefining the limits when measuring tortuosity in porous media. Phys Chem Chem Phys [Internet]. 2018 [cited 2018 Mar 12]; Available from: http://pubs.rsc.org/en/Content/ArticleLanding/2018/CP/C8CP00145F

38. Ahuja P, Sarkar R, Vasos PR, Bodenhausen G. Diffusion Coefficients of Biomolecules Using Long-Lived Spin States. J Am Chem Soc. 2009 Jun 10; 131(22):7498–9. https://doi.org/10.1021/ja902030k PMID: 19441812

39. Sarkar R, Vasos PR, Bodenhausen G. Singlet-State Exchange NMR Spectroscopy for the Study of Very Slow Dynamic Processes. J Am Chem Soc. 2007 Jan 1; 129(2):328–34. https://doi.org/10.1021/ja0647396 PMID: 17212412

40. DeVience SJ, Walsworth RL, Rosen MS. Dependence of nuclear spin singlet lifetimes on RF spin-locking power. Journal of Magnetic Resonance. 2012 May 1; 218(Supplement C):5–10. https://doi.org/10.1016/j.jmr.2012.03.016 PMID: 22578548

41. DeVience SJ, Walsworth RL, Rosen MS. Nuclear spin singlet states as a contrast mechanism for NMR spectroscopy. NMR Biomed. 2013; 26(10):1204–12. https://doi.org/10.1002/nbm.2936 PMID: 23606451

42. Pravdivtsev AN, Kozinenko VP, Hövener J-B. Only Para-Hydrogen Spectroscopy (OPSY) Revisited: In-Phase Spectra for Chemical Analysis and Imaging. J Phys Chem A. 2018 Nov 15; 122(45):8948–56. https://doi.org/10.1021/acs.jpca.8b07459 PMID: 30293421

43. Pileio G, Carravetta M, Levitt MH. Storage of nuclear magnetization as long-lived singlet order in low magnetic field. PNAS. 2010 Oct 5; 107(40):17135–9. https://doi.org/10.1073/pnas.1010570107 PMID: 20855584

44. DeVience SJ, Walsworth RL, Rosen MS. Preparation of Nuclear Spin Singlet States Using Spin-Lock Induced Crossing. Phys Rev Lett. 2013 Oct 22; 111(17):173002. https://doi.org/10.1103/PhysRevLett.111.173002 PMID: 24206484

45. Pravdivtsev AN, Kiryutin AS, Yurkovskaya AV, Vieth H-M, Ivanov KL. Robust conversion of singlet spin order in coupled spin-1/2 pairs by adiabatically ramped RF-fields. J Magn Reson. 2016 Dec 1; 273(Supplement C):56–64. https://doi.org/10.1016/j.jmr.2016.10.003 PMID: 27750072

46. Elliott SJ, Stevanato G. Homonuclear ADAPT: A general preparation route to long-lived nuclear singlet order. Journal of Magnetic Resonance. 2019 Apr 1; 301:49–55. https://doi.org/10.1016/j.jmr.2019.02.005 PMID: 30851665

47. Thrippleton MJ, Keeler J. Elimination of Zero-Quantum Interference in Two-Dimensional NMR Spectra. Angewandte Chemie International Edition. 2003 Aug 25; 42(33):3938–41. https://doi.org/10.1002/anie.200351947 PMID: 12949874

48. Pileio G, Ostrowska S. Accessing the long-time limit in diffusion NMR: The case of singlet assisted diffusive diffraction q-space. Journal of Magnetic Resonance. 2017 Dec 1; 285(Supplement C):1–7.

49. Sørensen OW, Eich GW, Levitt MH, Bodenhausen G, Ernst RR. Product operator formalism for the description of NMR pulse experiments. Prog Nucl Magn Reson Spectrosc. 1984 Jan 1; 16(Supplement C):163–92.

50. Aguilar JA, Adams RW, Duckett SB, Green GGR, Kandiah R. Selective detection of hyperpolarized NMR signals derived from para-hydrogen using the Only Para-hydrogen SpectroscopY (OPSY) approach. Journal of Magnetic Resonance. 2011 Jan 1; 208(1):49–57. https://doi.org/10.1016/j.jmr.2010.10.002 PMID: 21036636

51. Pileio G. Singlet NMR methodology in two-spin-1/2 systems. Progress in Nuclear Magnetic Resonance Spectroscopy. 2017 Feb 1; 98–99(Supplement C):1–19. https://doi.org/10.1016/j.pnmrs.2016.11.002 PMID: 28283084

52. Mamone S, Glöggler S. Nuclear spin singlet states as magnetic on/off probes in self-assembling systems. Phys Chem Chem Phys [Internet]. 2018 Aug 14 [cited 2018 Aug 22]; Available from: https://pubs.rsc.org/en/content/articlelanding/2018/cp/c8cp04448a

53. Levitt MH. Chapter 1 Long-lived States in Nuclear Magnetic Resonance: An Overview. In: Long-lived Nuclear Spin Order: Theory and Applications [Internet]. Royal Society of Chemistry; 2020 [cited 2020 Apr 16]. p. 1–32. (New Developments in NMR). Available from: https://doi.org/10.1039/9781788019972-00001

54. Puneet Ahuja, Riddhiman Sarkar, Vasos Paul R., Bodenhausen Geoffrey. Long-lived States in Multiple-Spin Systems. ChemPhysChem. 2009 Sep 2; 10(13):2217–20. https://doi.org/10.1002/cphc.200900335 PMID: 19630056

55. Shaka AJ, Keeler J, Frenkiel T, Freeman R. An improved sequence for broadband decoupling: WALTZ-16. Journal of Magnetic Resonance (1969). 1983 Apr 1; 52(2):335–8.

56. Klein MS, Almstetter MF, Schlamberger G, Nürnberger N, Dettmer K, Oefner PJ, et al. Nuclear magnetic resonance and mass spectrometry-based milk metabolomics in dairy cows during early and late lactation. J Dairy Sci. 2010 Apr; 93(4):1539–50. https://doi.org/10.3168/jds.2009-2563 PMID: 20338431

57. Strobel K, Hoff J van den, Pietzsch J. Localized proton magnetic resonance spectroscopy of lipids in adipose tissue at high spatial resolution in mice in vivo. J Lipid Res. 2008 Feb 1; 49(2):473–80. https://doi.org/10.1194/jlr.D700024-JLR200 PMID: 18024705

58. Pravdivtsev AN, Yurkovskaya AV, Petrov PA, Vieth H-M. Coherent evolution of singlet spin states in PHOTO-PHIP and M2S experiments. Phys Chem Chem Phys. 2017 Oct 4; 19(38):25961–9. https://doi.org/10.1039/c7cp04122e PMID: 28944791

59. Torres O, Procacci B, Halse ME, Adams RW, Blazina D, Duckett SB, et al. Photochemical Pump and NMR Probe: Chemically Created NMR Coherence on a Microsecond Time Scale. J Am Chem Soc. 2014 Jul 16; 136(28):10124–31. https://doi.org/10.1021/ja504732u PMID: 24945724

60. Jiang W, Lumata L, Chen W, Zhang S, Kovacs Z, Sherry AD, et al. Hyperpolarized 15N-pyridine Derivatives as pH-Sensitive MRI Agents. Sci Rep [Internet]. 2015 Mar 16 [cited 2019 May 20];5. Available from: https://www.ncbi.nlm.nih.gov/pmc/articles/PMC4360734/

61. Düwel S, Hundshammer C, Gersch M, Feuerecker B, Steiger K, Buck A, et al. Imaging of pH *in vivo* using hyperpolarized ^{13}C-labelled zymonic acid. Nat Commun. 2017 May 11; 8:15126. https://doi.org/10.1038/ncomms15126 PMID: 28492229

62. Eykyn TR, Kuchel PW. Scalar couplings as pH probes in compartmentalized biological systems: 31P NMR of phosphite. Magn Reson Med. 2003; 50(4):693–6. https://doi.org/10.1002/mrm.10580 PMID: 14523953

63. Farrell D, Miranda ES, Webb H, Georgi N, Crowley PB, McIntosh LP, et al. Titration_DB: Storage and analysis of NMR-monitored protein pH titration curves. Proteins: Structure, Function, and Bioinformatics. 2010; 78(4):843–57.

64. Bourgeois BF. Combination of valproate and ethosuximide: antiepileptic and neurotoxic interaction. J Pharmacol Exp Ther. 1988 Dec; 247(3):1128–32. PMID: 3144596

65. Bengs C, Sabba M, Jerschow A, H. Levitt M. Generalised magnetisation-to-singlet-order transfer in nuclear magnetic resonance. Physical Chemistry Chemical Physics [Internet]. 2020 [cited 2020 May 3]; Available from: https://pubs.rsc.org/en/content/articlelanding/2020/cp/d0cp00935k

66. Payne GS, Harris LM, Cairns GS, Messiou C, deSouza NM, Macdonald A, et al. Validating a robust double-quantum-filtered 1H MRS lactate measurement method in high-grade brain tumours. NMR Biomed. 2016 Oct; 29(10):1420–6. https://doi.org/10.1002/nbm.3587 PMID: 27514007

67. Shchepin RV, Barskiy DA, Coffey AM, Theis T, Shi F, Warren WS, et al. 15N Hyperpolarization of Imidazole-15N2 for Magnetic Resonance pH Sensing via SABRE-SHEATH. ACS Sens. 2016 Jun 24; 1 (6):640–4. https://doi.org/10.1021/acssensors.6b00231 PMID: 27379344